IEEE Access
Multidisciplinary ⋮ Rapid Review ⋮ Open Access Journal

Received 13 August 2023, accepted 2 October 2023, date of publication 10 October 2023, date of current version 16 October 2023.

Digital Object Identifier 10.1109/ACCESS.2023.3323247

RESEARCH ARTICLE

Enhancing Design and Performance Analysis of Satellite Entanglement-Based CV-QKD/FSO Systems

THANG V. NGUYEN[1], HOA T. LE[1], (Member, IEEE), HIEN T. T. PHAM[1], VUONG MAI[2], (Member, IEEE), AND NGOC T. DANG[1], (Member, IEEE)

[1]Wireless Systems and Applications Laboratory, Posts and Telecommunications Institute of Technology, Hanoi 100000, Vietnam
[2]Bradford-Renduchintala Centre for Space AI, University of Bradford, BD7 1DP Bradford, U.K.

Corresponding author: Ngoc T. Dang (ngocdt@ptit.edu.vn)

This work was supported by the Ministry of Information and Communications (Vietnam) under Grant DT.26/23. The work of Hoa T. Le was supported by the Asia Pacific Network Information Centre (APNIC) Foundation under the Switch! Project.

ABSTRACT Satellite QKD/FSO systems, which facilitate quantum key distribution (QKD) over free-space optical (FSO) links between satellites and ground stations, present a promising pathway toward achieving global security in upcoming sixth-generation (6G) wireless communications. Our study focuses on a superior type of these systems, the satellite EB/CV-QKD/FSO, which utilizes the continuous-variable (CV) method for quantum state representation and the entanglement-based (EB) scheme for QKD implementation. We propose the use of optical phase-shift keying (QPSK) signaling and dual-threshold/heterodyne detection (DT/HD) receivers to bolster the reliability and feasibility of satellite EB/CV-QKD/FSO systems. Closed-form expressions for key system performance metrics are derived using improved channel modeling. Numerical results are presented to showcase the effects of channel impairments on the system performance. We also provide recommendations for optimal system setup parameters, aiming to enhance performance.

INDEX TERMS Free-space optics (FSO), quantum key distribution (QKD), entanglement-based (EB) scheme, continuous-variable QKD (CV-QKD), optical phase-shift keying (QPSK) signaling, heterodyne detection (HD) receivers.

I. INTRODUCTION

The global deployment of 5G networks is underway, bringing substantial benefits to our economy, society, science, and education. However, traditional terrestrial networks alone can no longer fulfill the ever-growing demands for high-speed and reliable network access. The concept of non-terrestrial network (NTN) coordination has gained immense interest from both academia and industry to solve the limitations of coverage and capacity of terrestrial networks [1]. Among the various NTN solutions, satellite communications have emerged as a highly promising network architecture for the future sixth-generation (6G) wireless communications [2], [3].

The associate editor coordinating the review of this manuscript and approving it for publication was Hayder Al-Hraishawi.

In satellite-based 6G communications, the global storage and sharing of vast amounts of data and information necessitate robust security systems. An essential aspect of network security revolves around securely establishing the communication of secret keys among legitimate parties. In this regard, quantum key distribution (QKD) has been considered as a promising solution for achieving global security. Leveraging the principles of quantum physics, QKD enables the frequent and efficient sharing of secret keys between authorized entities, enabling the attainment of unconditional security [4], [5]. Since the initial proposal of the first QKD protocol by Kumarand and Garhwal in 1984, significant advancements have been made for long-distance transmissions using satellites and free-space optics (FSO) [6], [7]. An example of a satellite QKD/FSO system is shown in Fig. 1. A QKD/FSO system can be

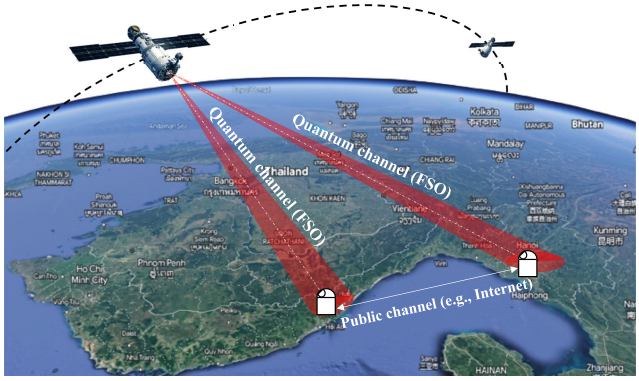

FIGURE 1. An example of satellite QKD/FSO system.

characterized by the way of representing quantum states and the role of satellites in implementing QKD.

In terms of representing the quantum states, two methods are commonly employed: discrete-variable (DV) QKD and continuous-variable (CV) QKD. In DV-QKD, quantum bits are encoded by utilizing discrete states of each photon, such as polarization or phase. On the other hand, CV-QKD allows for quantum bit encoding using properties of optical waves, such as intensity or phase (i.e., coherent states of light) [8], [9]. DV-QKD requires the use of single-photon detectors for detecting quantum bits. However, these detectors typically have low detection efficiency. In contrast, CV-QKD systems employing homodyne or heterodyne detection operate faster and more efficiently [8]. Furthermore, CV-QKD is compatible with standard optical communication technology as it can be implemented using readily available optical components [10].

The role of satellites is different depending on whether a prepare-and-measure (PM) or entanglement-based (EB) scheme is applied to implement QKD. In the PM scheme, the satellite serves as a trusted relay node for legitimate parties, such as Alice and Bob. The relay node facilitates the distribution of secret keys from Alice to Bob. The scheme requires multiple steps to distribute the key between Alice and Bob, resulting in increased complexity and inefficiency. In the EB scheme, the satellite acts as the central source and sends two beams of entangled quantum states to Alice and Bob simultaneously. This scheme enables independent measurements of received quantum states, facilitating the determination of the final secret key. Moreover, the scheme offers improved security, allowing two legitimate users to handle the secret key without the direct involvement of the satellite [11].

Different satellite QKD/FSO systems are formed by combining the QKD implementation scheme (PM or EB) with the method of representing quantum states (DV or CV). Extensive research has been conducted on satellite PM/CV-QKD/FSO systems [10], [12], [13], [14]. The first successful establishment of a satellite EB/DV-QKD/FSO system was achieved in 2017 [11]. However, investigations on satellite EB/CV-QKD/FSO have been relatively limited, despite the potential advantages of the entanglement-based QKD implementation and continuous-variable QKD. In a very recent study, a design concept for satellite EB/CV-QKD/FSO has explored using subcarrier intensity modulation/binary phase-shift keying (SIM/BPSK) and dual-threshold/direct detection (DT/DD) receiver [15]. However, it is worth noting that SIM/BPSK requires the use of additional RF subcarriers and large modulation depths, which can introduce issues of complexity and feasibility. On the other hand, DT/DD receivers, while straightforward, may suffer from low receiver sensitivity, which can impact the reliability of the system.

Another important issue is that the performance of satellite QKD/FSO systems is significantly influenced by various channel impairments, including atmospheric attenuation, atmospheric turbulence, and receiver noise. However, previous works on performance analysis in this context suffer from several limitations [10], [13], [15], [16]. Firstly, the impact of atmospheric attenuation is typically only considered within the troposphere layer, which extends up to an altitude of less than 20 km. Consequently, the influence of the stratosphere layer, which spans from 20 km up to 48 km above the Earth's surface [17], is often overlooked. Secondly, the atmospheric turbulence channel is commonly modeled using either Log-normal or Gamma-Gamma distributions. Nonetheless, recent experimental data suggest that the Fisher-Snedecor $\mathcal{F}$ distribution provides a better fit across weak to strong turbulence regimes compared to these two models [18]. Moreover, the effect of sun irradiance-induced receiver noise has not been taken into account in previous studies, despite its significance in practical scenarios [19]. Therefore, there is a need for further research to address these limitations and enhance the accuracy of performance analysis for satellite QKD/FSO systems.

In this study, our focus is on satellite EB/CV-QKD/FSO systems, which leverage the combined advantages of entanglement-based QKD implementation and continuous-variable QKD. Our primary objective is to enhance the reliability, feasibility, and performance analysis of the systems. This is achieved through the utilization of advanced techniques in encoding and decoding key information, comprehensive analysis, and optimization of system parameters. The key contributions of this paper can be summarized as follows:

- First, we propose the utilization of optical phase-shift keying (QPSK) signaling and dual-threshold/heterodyne detection (DT/HD) receivers as a means to enhance the reliability and feasibility of satellite EB/CV-QKD/FSO systems. Optical QPSK signaling offers several advantages, including the elimination of RF subcarriers and the ability to employ smaller modulation depths compared to SIM/BPSK. Additionally, the implementation of a DT/HD receiver improves receiver sensitivity compared to DT/DD, thereby reducing quantum bit errors. To the best of our knowledge, this study represents the

first proposal for incorporating optical QPSK signaling and DT/HD receivers in satellite EB/CV-QKD/FSO systems.

- Next, closed-form expressions of key performance metrics of satellite EB/CV-QKD/FSO systems, including quantum bit error rate (QBER), sift probability, and Eve's error probability, are derived by comprehensively considering the impacts of atmospheric attenuation, atmospheric turbulence, and receiver noise. To enhance the accuracy of channel modeling, atmospheric turbulence-induced fading modeled by the Fisher-Snedecor $\mathcal{F}$ distribution, atmospheric attenuation caused by both the troposphere and stratosphere layers, and sun irradiance-induced receiver noise are taken into account. This study represents the first instance where such comprehensive performance analysis is provided in the context of satellite EB/CV-QKD/FSO systems.
- Finally, we present numerical results that demonstrate the influence of different channel impairments on the performance of satellite EB/CV-QKD/FSO systems. Utilizing these results, we suggest appropriate values for crucial system setup parameters, including the receiver's aperture radius, the detector's threshold scale coefficient, and the transmit beam's divergence angle. By optimizing these parameter values to align with the specific channel conditions, we facilitate system designs and enhance overall performance.

The rest of the paper is organized as follows. In Section II, we describe the proposed satellite EB/CV-QKD/FSO system. Section III presents the channel model and the derivation of key performance metrics. Section IV focuses on discussing numerical results and optimizing system parameters. Finally, this paper is concluded in Section V.

II. SATELLITE EB/CV-QKD/FSO SYSTEM

In this section, we introduce our proposed EB/CV-QKD system. We start by presenting an overview of the conventional BBM92 QKD protocol. Subsequently, we describe our proposed BBM92 protocol and entanglement-based QKD system utilizing QPSK signaling and DT/HD receiver.

A. CONVENTIONAL BBM92 PROTOCOL

In 1992, Bennett et al. developed a QKD protocol without Bell's theorem, namely BBM92 [20]. The conventional protocol followed four steps:

1) At the source, Charlie (C) creates a stream of polarization-entangled photon pairs in the $|\psi\rangle = \frac{1}{\sqrt{2}}(|01\rangle + |10\rangle)$ state. These photon pairs are then split and sent to two legitimate parties, with one to Alice (A) and the other one to Bob (B).
2) After transmitting through free space, Alice and Bob can be applied one of two bases, either a rectilinear or diagonal, to measure each polarization-entangled photon. Therein, the rectilinear basis ($\oplus$) has a horizontal basis ($0°$) and a vertical basis ($\pi/2$), and the diagonal basis ($\otimes$) has two polarization states with ($\pi/2$, $-\pi/4$), respectively.
3) By using a public channel like the Internet, Alice and Bob publicly broadcast their measurement basis to each other. After communicating, they convert the remaining results by setting a rule of thumb for bit "0″ and bit "1″ to generate the sifted key as follows:

$$0 \rightarrow \begin{cases} 0 & if \quad \oplus \; was \; selected, \\ -\dfrac{\pi}{4} & if \quad \otimes \; was \; selected, \end{cases}$$
$$1 \rightarrow \begin{cases} \dfrac{\pi}{2} & if \quad \oplus \; was \; selected, \\ \dfrac{\pi}{4} & if \quad \otimes \; was \; selected. \end{cases}$$

All of the received photons, which have a different basis, are going to discard. This process is called **sifting process**. It is important to note that the measurement result should be anti-correlated, i.e., entangled photons; then Alice or Bob needs to invert her/his bits to get the same bit strings for both.
4) To obtain a final secure key, two legitimate parties, i.e., Alice and Bob, effectuate **information reconciliation** and **privacy amplification** procedures via the classical public channels.

B. PROPOSED BBM92 PROTOCOL

Similar to the operation of the BBM92 protocol, our proposed implementation is also in accordance with the four-step as follows:

Step 1: Charlie randomly selects one of two bases C_1 or C_2 to encode each binary bit onto one of two values of optical carrier (ϕ_C), where $\phi_C = (\phi_1 + \phi_2)/2$, is the combination of the phase from two branches of the Mach-Zehnder modulator (MZM). Four values of carrier's phase ϕ_A, known as phase states of QPSK signaling, are corresponding to four polarization states in the BBM92 protocol.

Step 2: At the receiver side, Alice and Bob mix their own signal phase, i.e., ϕ_U with $U \in \{A, B\}$, with received signal phase ϕ_C to form $\cos(\phi_C - \phi_U)$. Alice and Bob choose the value of ϕ_U randomly to either U_1 ($\phi_U = \pi/4$) or U_2 ($\phi_U = -\pi/4$). They pick the same basis as Charlie if Charlie chooses C_i and Alice and Bob use U_i, where $i \in 0, 1$. As a result, three random values (I_0, 0, and I_1), which are corresponding to bits "0″, "X″, and "1″, appear at the output current of the detector. Bit "X″ is discarded because Alice or Bob cannot detect the bit data based on the detection rule.

Step 3: At the time instants, Alice and Bob inform each other regarding the detected bit from the received signal through the public channel, i.e., the Internet. Discarded bits fall into one of the following two cases: (1) no bit is detected, and (2) generated bit values are unidentical bits. The rest of the bit sequence forms a new one, including the whole identical bits, called *sifted key*. Table 1 shows an example of our proposed protocol.

TABLE 1. An example of BBM92 protocol using QPSK signaling and DT/HD receiver.

Charlie (C)					Alice (A)					Bob (B)					Sifted key
Base	Bit	ϕ_1	ϕ_2	ϕ_C	Base	ϕ_A	$\phi_C-\phi_A$	I^A	Bit	Base	ϕ_B	$\phi_C-\phi_B$	I^B	Bit	
C_1	0	0	$\frac{\pi}{2}$	$\frac{\pi}{4}$	A_1	$\frac{\pi}{4}$	0	I_0	0	B_1	$\frac{-\pi}{4}$	$\frac{\pi}{2}$	0	X	X
C_1	0	0	$\frac{\pi}{2}$	$\frac{\pi}{4}$	A_2	$\frac{-\pi}{4}$	$\frac{\pi}{2}$	0	X	B_2	$\frac{\pi}{4}$	0	I_0	0	X
C_1	1	π	$\frac{3\pi}{2}$	$\frac{5\pi}{4}$	A_1	$\frac{\pi}{4}$	π	I_1	1	B_2	$\frac{\pi}{4}$	π	I_1	1	1
C_1	1	π	$\frac{3\pi}{2}$	$\frac{5\pi}{4}$	A_2	$\frac{-\pi}{4}$	$\frac{-\pi}{2}$	0	X	B_1	$\frac{-\pi}{4}$	$\frac{\pi}{2}$	0	X	X
C_2	0	0	$\frac{-\pi}{2}$	$\frac{-\pi}{4}$	A_1	$\frac{\pi}{4}$	$\frac{-\pi}{2}$	0	X	B_2	$\frac{\pi}{4}$	$\frac{-\pi}{2}$	0	X	X
C_2	0	0	$\frac{-\pi}{2}$	$\frac{-\pi}{4}$	A_2	$\frac{-\pi}{4}$	0	I_0	0	B_1	$\frac{-\pi}{4}$	0	I_0	0	0
C_2	1	π	$\frac{\pi}{2}$	$\frac{3\pi}{4}$	A_1	$\frac{\pi}{4}$	$\frac{\pi}{2}$	0	X	B1	$\frac{-\pi}{4}$	π	I_1	1	X
C_2	1	π	$\frac{\pi}{2}$	$\frac{3\pi}{4}$	A_2	$\frac{-\pi}{4}$	π	I_1	1	B_2	$\frac{\pi}{4}$	$\frac{\pi}{2}$	0	X	X

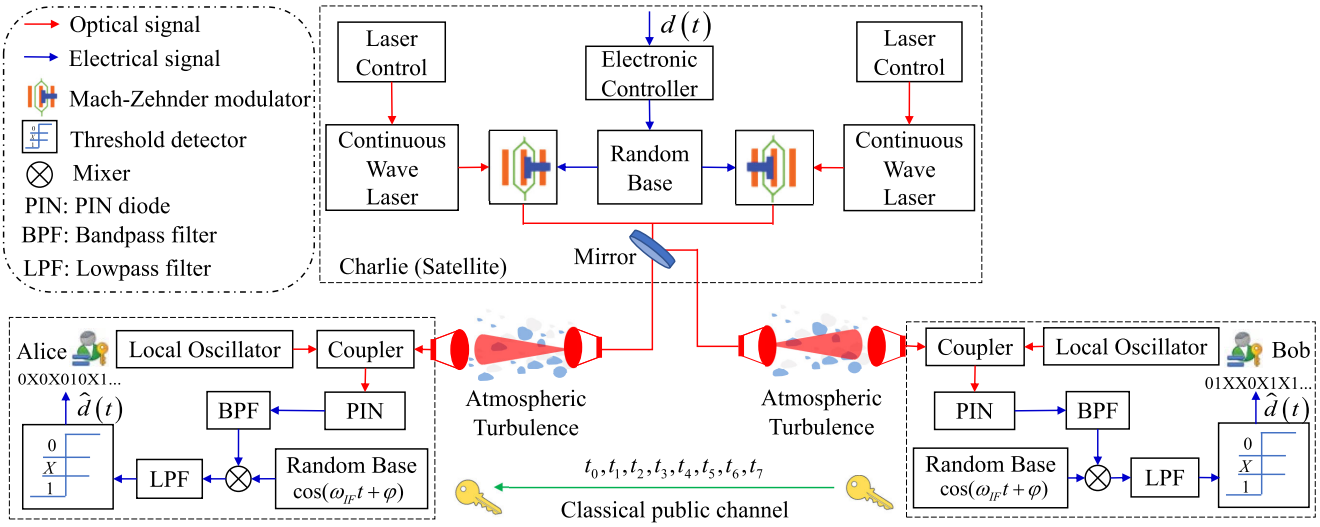

FIGURE 2. Entanglement-based QKD system using QPSK signaling and DT/HD receiver.

Step 4: Finally, two procedures, including information reconciliation and privacy amplification, are further handled as in step 4 of the BBM92 protocol to create a final secret key without error.

C. PROPOSED ENTANGLEMENT-BASED QKD SYSTEM

Figure 2 illustrates the block diagram of entanglement-based QKD systems for global security, including three parties: Charlie (satellite) and Alice and Bob (two legitimate users located at the ground). In the duration of the preparation stage, Charlie, Alice, and Bob are assumed perfect pre-synchronization by using a global positioning system (GPS). Source and destinations are connected via the FSO channel.

At the source, Charlie's raw key, denoted as $d(t)$, is first modulated by an MZM to create the electrical pulses. At each branch, the phase of the optical carrier is governed by the bit "0″ or bit "1″ as shown in Tab. 1. The random base module randomly picks one of two MZMs corresponding to two bases C_1 and C_2 to encode the binary data using the phase of a continuous-wave optical carrier, facilitated by a QPSK modulator. Following this, an optical beam splitter splits the optical signal into two beams with identical phases. One of these beams is transmitted to Alice while the other is transmitted to Bob.[1] Four different values of ϕ_C correspond to four phase states of the QPSK signaling scheme. As a result, the output signal of the source (Charlie) is given as

$$I_{Tx} = \sqrt{P_t}\exp\left[i(2\pi f_c t + \phi_C)\right], \tag{1}$$

where P_t is the transmitted power and f_c is the optical carrier frequency.

At the receiver sides (Alice and Bob), the telescope collects the optical beam; the received signal can be expressed as

$$I_{Rx} = \sqrt{P_r}\exp\left[i(2\pi f_c t + \phi_U)\right], \tag{2}$$

where $P_r = P_t h$ is the received power, in which h is the channel coefficient, which is described in more detail in the next part. Besides, the optical signal created by the LO can be shown as

$$I_{LO} = \sqrt{P_{LO}}\exp\left[i(2\pi f_{LO} t)\right], \tag{3}$$

where P_{LO} and f_{LO} are the power and the frequency of the LO, respectively. After that, the received signals are combined with a continuous wave generated by the local oscillator.

[1] It is worth noting that the quantum correlation can be achieved thanks to the conversation between Alice and Bob via the classical public channel to notify each other the time instants that they all detect bit "0″ or bit "1″.

Thanks to the PIN photodiode, the optical signal is converted to the electrical signal, which can be written as

$$I_p \propto \Re I_{Rx} + I_{LO}|^2 \propto \Re\left\{(P_r + P_{LO}) + 2\sqrt{P_r P_{LO}}\cos\left(2\pi f_{IF} t + \phi_C\right)\right\} + i_n, \tag{4}$$

where $f_{IF} = f_c - f_{LO}$ is the intermediate frequency. $\Re$ is the responsivity of the PIN. i_n denotes the noise current. The bandpass filter (BPF) is used to get rid of undesired signals. After that, the useful component of intermediate frequency is multiplied with the reference signal $\cos(2\pi f_{IF} t + \phi_U)$ of the receiver's random base component. Hence, the decoded current can be determined as

$$\begin{aligned} I_F &= 2\Re\sqrt{P_r P_{LO}}\cos\left(2\pi f_{IF} t + \phi_C\right)\cos\left(2\pi f_{IF} t + \phi_U\right) + i_n, \\ &= \Re\sqrt{P_r P_{LO}}\cos\left(4\pi f_{IF} t + \phi_C + \phi_U\right) \\ &+ \Re\sqrt{P_r P_{LO}}\cos\left(\phi_C - \phi_U\right) + i_n. \end{aligned} \tag{5}$$

Two decoded bases of each legitimate user are randomly selected by setting the phase of the reference signal. Then, the low-pass filter (LPF) is utilized to eliminate the undesired component ($4f_{IF}$). Consequently, the bit "1″ and bit "0″ are decided by a threshold detector and can be expressed as

$$I = \Re\sqrt{P_r P_{LO}}\cos\left(\phi_C - \phi_U\right) + i_n. \tag{6}$$

Under the effect of noise, the detection rule can be expressed as

$$\text{Decision rule} = \begin{cases} 1 & \text{if } (I \le d_1) \\ 0 & \text{if } (I \ge d_0) \\ X & \text{if otherwise} \end{cases} \tag{7}$$

where d_0 and d_1 are the thresholds to detect bit "0″ and "1″, respectively (see [21] and the reference therein for more detail). X denoted as no bit is generated.

The security of QPSK-based QKD is ensured thanks to the random base at legal receivers (i.e., Alice and Bob), which choose their phase (i.e., ϕ_U) randomly to combine with the phase of the signal received from Charlie (i.e., ϕ_C). The eavesdropper (Eve) can only detect a bit of the quantum key when its phase matches to $(\phi_C - \phi_U)$ and Alice and Bob use the same value of ϕ_U. Besides, the difference in channel characteristics and noise variance among the links, i.e., Charlie-to-Alice, Charlie-to-Bob, and Charlie-to-Eve, also helps to enhance the security. This difference reduces the probability that Alice, Bob, and Eve detect the same value of the quantum bit.

III. SYSTEM PERFORMANCE ANALYSIS

In this section, we present channel model and closed-form expressions for key performance metrics of the satellite EB/CV-QKD/FSO system. Assuming that a fine tracking system with perfect alignment is deployed and the phase lock loop is implemented to compensate for the effect of phase noise [22]. In addition, we ignore the effect of the frequency mismatch because the current receiver design for satellite-based CV-QKD/FSO communication systems can deal with the frequency shift up to ±14 GHz [23], [24].

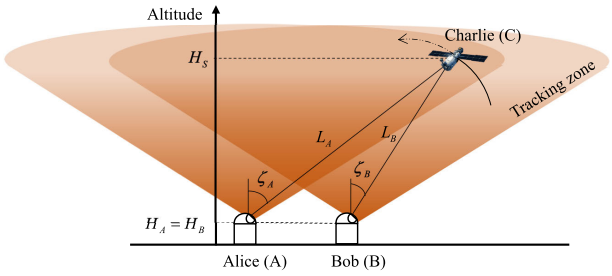

FIGURE 3. Schematic illustration of considered system for performance analysis.

A. CHANNEL MODEL

Various factors affect to the optical channel during propagation from the satellite to two legitimate users on the ground. As shown in Fig. 3, depending on the geography area, an existing minimum elevation angle of the base station can be determined to see satellites in LEO orbit, e.g., the range of the elevation angle in Japan from 30° to 150° [15]. In the tracking zone, the entanglement-based QKD system performance is evaluated by taking into account three main effects, including atmospheric attenuation, h_a, geometric spreading loss, h_g, and turbulence-induced fading, h_t.

1) ATMOSPHERIC ATTENUATION

The quantum signal attenuates while propagating from the satellite to Alice and Bob because the composition of gas molecules and aerosol particles in the air absorbs the laser beam energy and changes the light direction. Before coming to the ground, the optical signal propagates through three environmental conditions, including vacuum condition, stratosphere condition, and troposphere condition. Therein, the effect of vacuum conditions on the quantum signal is ignored. The troposphere layer is the region's strongest effect on the optical signal due to aerosol in the air. In addition, active volcanoes have recently occurred more frequently and produced aerosols during active. These aerosols are ejected from volcanoes into the stratosphere layer and then spread worldwide in a few weeks [17]. This results in the optical signal being affected when passing through this medium. Therefore, it is necessary to consider the effect of the stratosphere on optical signals from satellites. As a function of transmission distance, the Beer-Lambert law is utilized to estimate the path loss through two-atmosphere layers h_a as follows [17], [22]

$$h_a = h_l h_s = \exp\left(-\sigma_{tr} L\right)\exp\left(-\sigma_{st} H_{st}\sec(\xi)\right), \tag{8}$$

where h_l and h_s are denoted as troposphere attenuation coefficient and stratosphere attenuation coefficient, respectively. $L = (H_s - H_U)/\cos(\xi)$ is the propagation length of the FSO link in which ξ is the satellite's zenith angle. σ_{tr} and σ_{st} are the attenuation coefficient of the troposphere layer (the

TABLE 2. Attenuation coefficient for different atmospheric layers.

Attenuation coefficient	Troposphere layer σ_{tr} (km^{-1})	Heavy fog	28.75
		Light fog	4.6
		Haze	0.966
		Clear air	0.0989
	Stratosphere layer σ_{st} (km^{-1})	Extreme volcanic	10^{-1}
		High volcanic	2×10^{-2}
		Moderate volcanic	8×10^{-4}
		Background volcanic	10^{-4}

altitude of 20 km above Earth's surface) and the stratosphere layer (the altitude of 20 to 48 km above Earth's surface). H_{st} is the vertical extent of the stratosphere layer. Table 2 shows the values of σ_{tr} and σ_{st} at the optical wavelength of $\lambda = 1550$ nm [17].

2) GEOMETRIC LOSS

From the satellite, the optical beam, which is considered a Gaussian beam, is transmitted to the ground via the free-space channel. Due to the long-distance transmission, the beam spreads out; then the fraction of the collected power at the ground can be determined as

$$h_g \approx A_0 \exp\left(-\frac{2r^2}{w_{Leq}^2}\right), \tag{9}$$

where $A_0 = [\mathrm{erf}(v)]^2$ is the fraction of the collected power at $r = 0$, i.e., Alice and Bob can be situated at the center of the Gaussian beam footprint. The equivalent beam-waist can be calculated as $w_{Leq}^2 = w_z^2 \frac{\sqrt{\pi}\mathrm{erf}(v)}{2v\exp(-v^2)}$. $v = (\sqrt{\pi D_r/2})/(\sqrt{2}w_L)$ is the ratio between the aperture detector radius and the beamwidth. At a distance L, the beam-waist, denoted as w_z, can be approximated as $w_z \approx w_0\sqrt{1+\epsilon\left(\frac{\lambda L}{\pi w_0^2}\right)^2}$ in which $w_0 = (2\lambda)/(\pi\theta)$ is the beam-waist at distance $L = 0$ and θ is the divergence angle. $\epsilon = (1 + 2w_0^2/\rho_0^2(L))$, and $\rho_0(L) = (0.55C_n^2(L)k^2L)^{-3/5}$ is the coherence length [25].

3) ATMOSPHERIC TURBULENCE-INDUCED FADING

The ability of atmospheric turbulence to effectively mix air with various characteristics is what gives it its significance in meteorology as well as communication from space. Local fluctuations in the refractive index occur as light travels from the emitter to the photoreceptor due to the inhomogeneity of temperature and pressure in the atmosphere; these variations considerably impair the performance of the quantum channel. Accurately simulating atmospheric turbulence under varied situations is one of the most crucial tasks in efforts to reduce the erosion of optical communication system performance. Aside from the Log-normal, Gamma-Gamma distribution is normally used to model the turbulence-induced fading; in this study, the composite turbulent coefficient follows a Fisher-Snedecor $\mathcal{F}$ distribution and is expressed as [26]

$$f_{h_t}(h_t) = \frac{a^a(b-1)^b h_t^{a-1}}{\mathcal{B}(a,b)(ah_t+b-1)^{a+b}}, \tag{10}$$

where $\mathcal{B}(\cdot)$ is the beta function while the parameters a and b of $\mathcal{F}$-distribution is given as [18]

$$a = \frac{1}{\exp\left(\sigma_{\ln\mathcal{S}}^2\right) - 1}, \tag{11}$$

$$b = \frac{1}{\exp\left(\sigma_{\ln\mathcal{L}}^2\right) - 1} + 2, \tag{12}$$

where $\sigma_{\ln\mathcal{S}}^2$ and $\sigma_{\ln\mathcal{L}}^2$ are the corresponding small-scale and large-scale log-irradiance variances, which can be determined via Rytov variance (σ_R^2) as shown in [27]. σ_R^2 defines weak, moderate, and strong turbulence corresponding to $\sigma_R^2 < 1$, $\sigma_R^2 \approx 1$, and $\sigma_R^2 > 1$. In the case of plane wave propagation, the Rytov variance, denoted by σ_R^2, is given as [27] and can be shown as

$$\sigma_R^2 = 2.25k^{7/6}\sec^{11/6}(\xi_i)\int_{H_v}^{H_j} C_n^2(h)(h-H_v)^{5/6}dh, \tag{13}$$

where σ_R^2 for the i-th path can be written as a function of $\sigma_R^2 = f\left(\xi_i, H_v, H_j\right)$ with ξ and H represent for zenith angle and altitude, respectively. Additionally, $C_n^2(h)$ is the variation of the refractive index structure parameter described by the Hufnagel-Valley model [28, (19)] and can be expressed as

$$C_n^2(h) = 0.00594\left(\frac{v_{\mathrm{wind}}}{27}\right)^2\left(10^{-5}h\right)^{10}\exp\left(-\frac{h}{1000}\right) + 2.7\times10^{-16}\exp\left(-\frac{h}{1500}\right) + C_n^2(0)\exp\left(-\frac{h}{100}\right), \tag{14}$$

where $C_n^2(0)$ is the ground level turbulence, and v_{wind} (m/s) is the root mean squared wind speed.

B. SIFT PROBABILITY

In this section, the mathematical closed-form expressions of each security performance metric are derived. When compared to integral expressions, closed-form expressions have the potential to offer a clearer understanding of how various design variables influence performance. Moreover, there exist particular integrals that are intractable. They cannot be used to compute results. Regarding the simulation, achieving precise results demands a significant number of simulation runs. As a result, the simulation process can be highly time-consuming. Closed-form expressions could substantially alleviate the computational time required. Here, closed-form expressions help to identify the secure performance of satellite entanglement-based CV-QKD/FSO systems as a function of many parameters including the altitude of the satellite, optical wavelength, divergence angle, zenith angle, wind speed, detector responsivity, etc., and other parameters as shown in Table 3.

1) SIFT PROBABILITY BETWEEN CHARLIE AND ALICE/BOB

Sift probability, P_{sift}, is defined as the probability that two legitimate users (Alice and Bob) can decode bits using dual-threshold detection. In the entanglement-based QKD system,

TABLE 3. System parameters.

Name	Symbol	Value
LEO satellite altitude	H_{SAT}	600 km
Alice/Bob's station high	H_U	10 m
Optical wavelength	λ	1550 nm
Divergence angle	θ	0.4 mrad
Zenith angle	ξ	30°
Threshold scale coefficient	ρ	2
Sun's spectral irradiance	ω_r	0.2 kW/m$^2\mu$m
Wind speed	v_{wind}	21 m/s
Turbulence strength	C_n^2	10^{-13} m$^{-2/3}$
Optical bandwidth	B_0	250 Ghz
Bit rate	R_b	1 Gbps
Aperture radius	D_r	5 cm
Transmitted power	P_t	5 dBm
Local oscillator power	P_{LO}	−5 dBm
Electron charge	q	1.6×10^{-19}
Dark current	I_d	3×10^{-9} A
Boltzamann's constant	k_B	1.38×10^{-23} J/K
Receiver temperature	T	298 K
Detector responsivity	$\Re$	0.8
Load resistance	R_L	50 Ω

the sift probability can be calculated as

$$P_{\text{sift}}^{CAB} = P_{C,U}(0,0) + P_{C,U}(0,1) + P_{C,U}(1,0) + P_{C,U}(1,1), \tag{15}$$

where $P_{C,U}(x,y)$ in which $(x,y) \in \{0,1\}$ is the probability that bit "x" sent by Charlie coincides with the decoded bit "y" of Alice and Bob. Then, the probability $P_{C,U}(x,y)$ can be calculated as

$$P_{C,U}(x,y) = P_C(x)P_{U|C}(y|x), \tag{16}$$

where $P_C(x)$ is the probability that satellite transmits bit "x". $P_{U|C}(y|x)$ is the conditional probability that Alice and Bob detect bit "y" when Charlie send bit "x" and can be determined as

$$P_{U|C}(0|x) = \int_0^\infty Q\left(\frac{i_x^U - d_0^U}{\sigma_N^U}\right) f_{h_t^U}\left(h_t^U\right) dh_t^U, \tag{17}$$

$$P_{U|C}(1|x) = \int_0^\infty Q\left(\frac{d_1^U - i_x^U}{\sigma_N^U}\right) f_{h_t^U}\left(h_t^U\right) dh_t^U, \tag{18}$$

where $i_0^U = -i_1^U = -\Re\sqrt{P_r P_{LO}}$, $d_0^U = \rho I_0^U$ and $d_1 = \rho I_1^U$ with ρ is threshold scale coefficient. $Q(\cdot)$ is the Gaussian Q-function. σ_N^U is the total noise variance, where the shot noise is given as [29]

$$\sigma_N^U = 2q(\Re P_{LO} + \Re P_b + I_d)\Delta f + \frac{4k_B T}{R_L}\Delta f, \tag{19}$$

where q is the electron charge, T is the absolute temperature, I_d is the dark current, R_L is the load resistance, k_B is the Boltzmann's constant, and $\Delta f = \frac{R_b}{2}$ is the efficient bandwidth with bit rate R_b. $P_b = \Omega_r \pi D_r^2 \Delta\lambda$ is the background noise power collected at user U's receivers, Ω_r is the Sun's spectral irradiance above Earth, $\Delta\lambda = \frac{B_0\lambda^2}{c}$, B_0 is the optical bandwidth, λ is the optical wavelength, c is the speed of light. In this work, the signal-dependent shot noise contributed from the received signal is ignored due to its power being much lower than the local oscillator power.

To solve the integral (17) and (18), we first use the conversion between Q function and erfc function, i.e., $Q(x) = \frac{1}{2}\text{erfc}\left(\frac{x}{\sqrt{2}}\right)$, then expressing erfc function as Meijer G-function, i.e., $\text{erfc}(\sqrt{x}) = \frac{1}{\sqrt{\pi}} G_{1,2}^{2,0}\left(x \middle| \begin{matrix} 1 \\ 0 \ 1/2 \end{matrix}\right)$ [30, Eq. (06.27.26.0006.01)]. By using [31, Eq. (8.4.2.5)] and [32, Eq. (21)], and after several mathematical manipulations, the closed-form of (17) can be derived as in (20), shown at the bottom of the page, where $\mathcal{A} = \frac{\Re(1+\rho)\sqrt{P_t P_{LO} h_a h_g}}{\sigma_N^U}$. It is worth noting that Eq. (18) can be similarly solved with Eq. (17). Therefore, to keep the paper concise, we did not show the closed-form of Eq. (18).

2) SIFT PROBABILITY BETWEEN ALICE AND BOB

Similar to calculating the sift probability above, the P_{sift} between Alice and Bob can be expressed as

$$P_{\text{sift}}^{AB} = P_{A,B}(0,0) + P_{A,B}(0,1) + P_{A,B}(1,0) + P_{A,B}(1,1), \tag{21}$$

where $P_{A,B}(x,y)$ is the probability that Alice's detect bit "x" coincides with Bob's detected bit "y". And, the probability $P_{A,B}$ can be given as

$$\begin{aligned} P_{A,B}(x,y) = {} & P_C(x)P_{A|C}(x|x)P_{B|C}(y|x) \\ & + P_C(y)P_{A|C}(x|y)P_{B|C}(y|y). \end{aligned} \tag{22}$$

C. QUANTUM BIT ERROR RATE

In the entanglement-based QKD system, the quantum bit error rate (QBER) reflects the probability of bit error in the sifted key. In optical systems, these bit errors are normally on the order of a few percent [33]. In the considered system, the QBER can be expressed as [34]

$$\text{QBER} = \frac{P_e}{P_{sift}}, \tag{23}$$

where P_e is the probability that shows how many bit errors in the sifted key are caused by environmental conditions and/or Eve's intervention. In our system, the P_e is determined in two cases as followed

$$P_{U|C}(0|x) = \frac{\mathcal{A}^{-2a}a^a}{2^{1-a}(b-1)^a\sqrt{\pi}\mathcal{B}(a,b)\Gamma(a+b)} G_{3,2}^{1,3}\left[\frac{2a}{\mathcal{A}^2(b-1)}\middle| \begin{matrix} 1-(a+b) & 1-a & \frac{1}{2}-a \\ 0 & & -a \end{matrix}\right]. \tag{20}$$

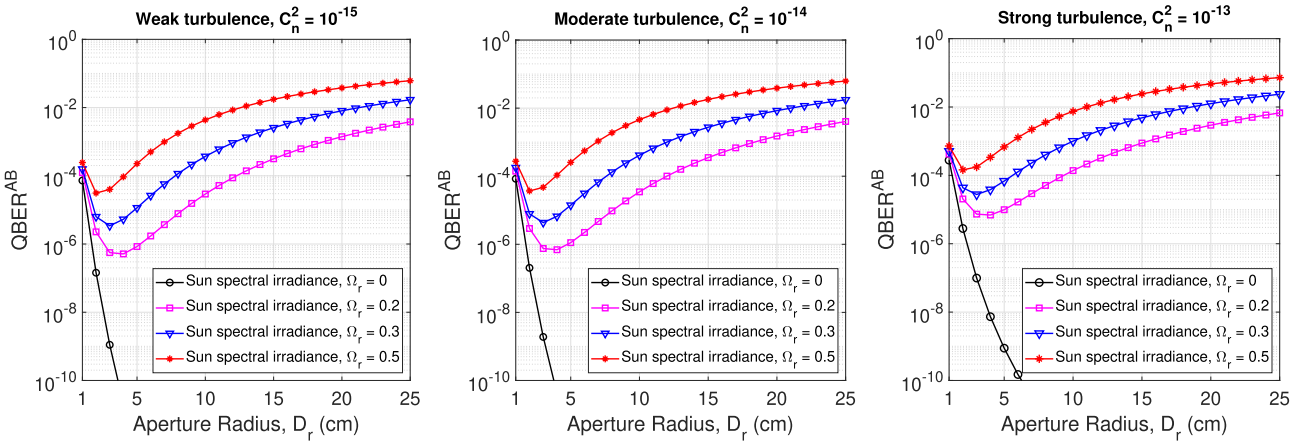

FIGURE 4. Alice's/Bob's QBER in different turbulence conditions and the sun's spectral irradiance.

QBER for the key transmission between Charlie and two legitimate users

$$\text{QBER}^{CAB} = P_{C,U}(0,1) + P_{C,U}(1,0), \tag{24}$$

in which $P_{C,U}(.)$ is the probability that presents the bit sent from Charlie (satellite) is different from the received bits at Alice and Bob.

QBER for the key transmission between Alice and Bob

$$\text{QBER}^{AB} = P_{A,B}(0,1) + P_{A,B}(1,0), \tag{25}$$

in which $P_{A,B}(,)$ denotes the probability that the received bits at two legitimate users are not the same.

D. EVE'S ERROR PROBABILITY

To investigate the security of the proposed CV-QKD system, we consider the eavesdropping attack, where the eavesdropper (i.e., Eve) tries to detect the quantum key that Charlie sends to Alice and Bob. The most practical attacking strategy for Eve is by locating its unauthorized receiver within the beam footprint near Alice's of Bob's receiver since the optical beam experiences geometric spreading. Assuming that Eve's location is at the distance of r_E from the center of the beam footprint, where Alice/Bob is located. We consider the case that Eve uses the optimal threshold ($d_t^E = 0$) to detect Charlie's data. If Eve is wrong to receive the bit sent from the satellite, it is called Eve's error probability and can be determined as

$$\begin{aligned} P_{\text{error}}^E &= P_{C,E}(0,1) + P_{C,E}(1,0), \\ &= P_C(0)P_{E|C}(1|0) + P_C(1)P_{E|C}(0|1), \end{aligned} \tag{26}$$

where $P_{C,E}(0,1)$ and $P_{C,E}(1,0)$ are the joint probabilities that Eve falsely detects the bit sent from Charlie. $P_C(x)$ and $P_{E|C}(y|x)$ are the probability of Charlie sent bit "x" and the conditional probabilities that Eve detects bit "y" instead of bit "x". That probability can be calculated as

$$P_{E|C}(1|0) = \int_0^\infty Q\left(\frac{d_t^E - i_0^E}{\sigma_N^E}\right) f_{h_t^E}\left(h_t^E\right) dh_t^E, \tag{27}$$

$$P_{E|C}(0|1) = \int_0^\infty Q\left(\frac{i_1^E - d_t^E}{\sigma_N^E}\right) f_{h_t^E}\left(h_t^E\right) dh_t^E, \tag{28}$$

where $i_0^E = -i_1^E = -\Re\sqrt{P_t h_a^E h_g^E h_t^E P_{LO}^E}$ denote the current received signal of the attacker, i.e., Eve. Therein, h_a^E,h_g^E, and h_t^E correspond to the atmospheric attenuation, geometric spreading loss, and turbulence-induced fading, which are introduced in Section 2. As demonstrated in [35], the fading channel at Eve's location is uncorrelated with the position of Alice and Bob if the distance between Eve and Alice or Eve and Bob is in the order of tens meters.

IV. RESULTS AND DISCUSSIONS

In this section, we discuss selected numerical results to demonstrate the advantages of our proposed EB/CV-QKD system. The parameters used in the analysis, unless otherwise noted, are given in Table 3.

First, we are interested in the performance of the key transmission from Charlie to Alice and Bob; then, the QBER^{AB} is investigated in three turbulence-induced fading conditions as shown in Fig. 4, including a weak regime with $C_n^2 = 10^{-15}$, a moderate regime with $C_n^2 = 10^{-14}$, and a strong regime with $C_n^2 = 10^{-13}$. In this result, we consider the impact of an important parameter which is the sun's spectral irradiance denoted as Ω_r, due to the fact that it directly affects key transmission. Besides, we examine QBER^{AB} over the range of the aperture radius with the purpose of finding a suitable radius for the design of the receiver. In the condition of $\Omega = 0$, i.e., there is no sun spectral irradiance, the QBER^{AB} obviously decreases when the size of the aperture radius increases. This is because the increase of the aperture radius helps to obtain more received power. However, the use of an aperture with a large radius is

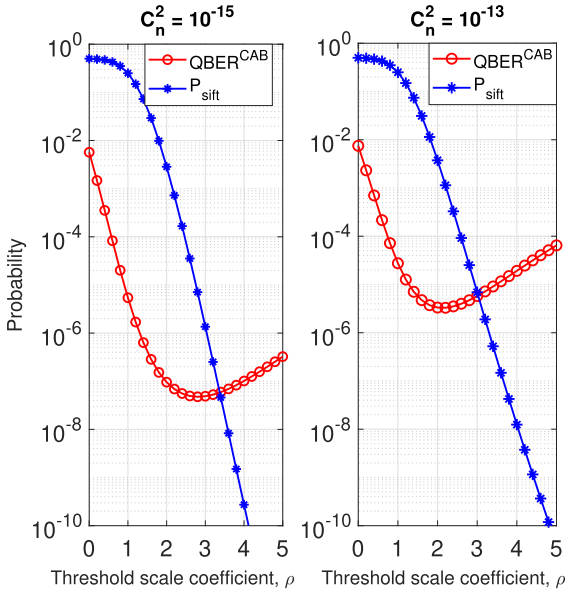

FIGURE 5. Alice's/Bob's *QBER* Alice/Bob and P_{sift} versus the threshold scale coefficient, denoted as ρ, in weak and strong turbulence regimes.

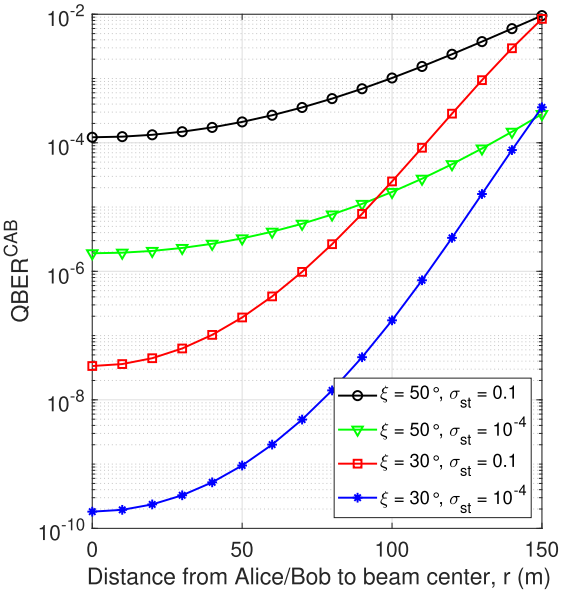

FIGURE 6. Effect of the stratosphere layer on *QBER*^{CAB} over the range of the distance from Alice/Bob to the beam center.

not a good choice when there is exist of the sun's spectral irradiance. The reason can be explained through Eq. (19). The sun's spectral irradiance-induced background power collected at Alice's/Bob's receiver grows up proportional to the square of the receiver's radius. Based on the minimum values of QBER^{AB} shown this figure, the aperture radius is recommended as $D_r = 2$ cm, $D_r = 3$ cm, and $D_r = 4$ cm corresponding to three sun's spectral conditions as $\Omega_r = 0.2$ kW/m$^2\mu$m, $\Omega_r = 0.3$ kW/m $^2\mu$m, and $\Omega_r = 0.5$ kW/m$^2\mu$m.

Two performance metrics, including the sift probability, P_{sift}, and quantum bit error rate, $QBER^{CAB}$, are investigated in Fig. 5 in weak and strong turbulence conditions. In a non-entanglement-based QKD system using QPSK [21], the probability that Alice/Bob detects incorrect bit "0″ or "1″ reduces when the difference between two thresholds d_0 and d_1 is large, i.e., the large value of the threshold scale coefficient (ρ). However, this conclusion is not always true in entanglement-based QKD systems using QPSK. As seen from the figure for the strong turbulence regime, the $QBER^{CAB}$ curve goes down when ρ increases from 0 to 2. It then grows up with $\rho > 2$. The reason can be found in Eq. (23). $QBER^{CAB}$ depends on both the probability of bit errors in the sifted key and the sift probability. When ρ increases from 0 to 2, the increase of ρ helps to decrease the false detection as the thresholds to detect bit "0″ and "1″ are more separate. However, in the regime of $\rho > 2$, the sift probability still reduces fast while the probability of bit errors is stable. Consequently, $QBER^{CAB}$ tends to rise. Therefore, the threshold scale coefficient smaller than 2 is recommended to ensure low *QBER* and high sift probability, which guarantees a high key rate.

The relationship between $QBER^{CAB}$ and the distance from Alice/Bob to the beam center is examined in Fig. 6. In this result, we consider two values of the zenith angle with $\xi = 30°$ and $\xi = 50°$ in different stratosphere layer conditions, i.e., extreme volcanic with $\sigma_{st} = 0.1$ and background volcanic with $\sigma_{st} = 10^{-4}$. As shown in Table 3, the divergence angle is set at 0.4 mrad; then, the equivalent beamwidth at Alice's/Bob's location is approximately 187 meters. Obviously, the $QBER^{CAB}$ will be high if the receiver, unfortunately, situates at the edge of the beam footprint because the received power is low due to the properties of the Gaussian beam. In addition, the influence of the stratosphere layer is clearly illustrated in this result. Notably, in the center of the beam footprint, i.e., $r = 0$, and using the same zenith angle, the $QBER^{CAB}$ is 1.44×10^{-6} in the extreme volcanic condition while it is 7.39×10^{-9} in the case of the background volcanic. To cope with the impact of the stratosphere layer, we can design the zenith angle to improve performance. For instance, to maintain $QBER^{CAB} < 10^{-6}$ with $\sigma_{st} = 10^{-4}$, the zenith angle should decrease, e.g., 30°.

Figure 7 shows the relationship between Eve's error probability, P^E_{error}, and the divergence angle. As defined in the previous section, r_E is the distance from Eve's location to Alice's/Bob's one. In this result, we consider five Eve's locations corresponding to 80, 100, 120, 140, and 160 meters. Following the increasing trend of the divergence angle, the P^E_{error} seem to decrease until getting the optimal point. After that, Eve's error probability rises up due to the property of the optical Gaussian beam. Obviously, it is easier for Alice/Bob to track the signal from Charlie by selecting the large value of the divergence angle; however, it also leads to an increase in the bit error rate at the receiver side [36]. Using a small value of divergence angle results in not only low $QBER^{CAB}$ but also P^E_{error}. As reported in [15], the P^E_{error} of 0.1 is high enough for entanglement-based QKD transmitter design.

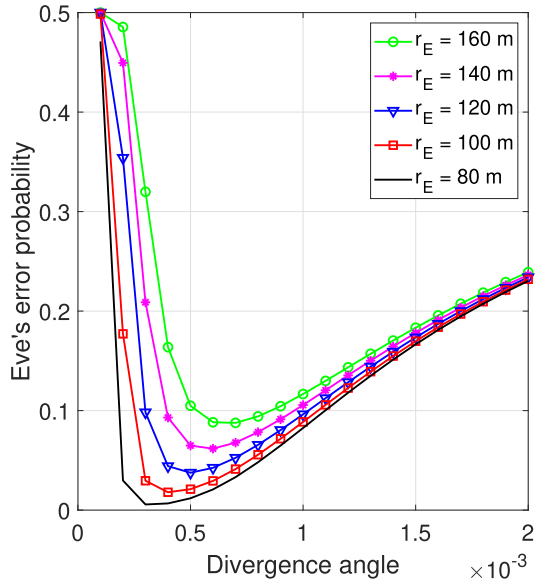

FIGURE 7. The relationship between Eve's error probability and divergence angle at different Eve's locations.

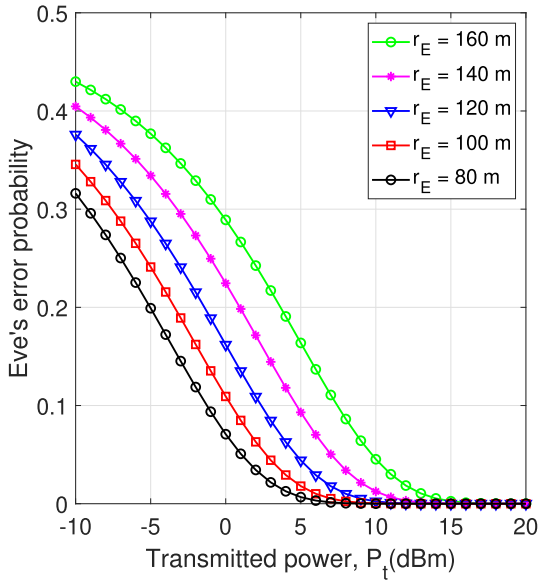

FIGURE 8. Eve's error probability versus Charlie's transmitted power in different of Eve's locations.

Therefore, with the divergence angle of 0.4 mrad, the safe zone for our proposed QKD system is 140 m around Alice/Bob, where P^E_{error} is higher than 0.1.

In terms of security property, we always wish the error probability of the attacker, i.e., Eve, as high as possible. Or in other words, the attacker always aims to get close to legitimate users so that they can tap information from the transmitters. Therefore, we investigate Eve's error probability, P^E_{error}, versus Eve's locations, i.e., r_E, over the range of the transmitted power from Charlie, P_t, from -10 dBm to 20 dBm. To guarantee P^E_{error} is high enough, e.g., $P^E_{\text{error}} = 0.1$, Charlie should limit his transmitted power below -1.13, 0.41, 2.37, 4.72 and 7.43 dBm corresponding to Eve's locations of 80 m, 100 m, 120 m, 140 m, and 160 m, correspondingly.

V. CONCLUDING REMARKS

This study has focused on satellite EB/CV-QKD/FSO systems, which utilize the combined benefits of entanglement-based QKD implementation and continuous-variable QKD. We have proposed the use of optical QPSK signaling and DT/HD receivers to enhance the reliability and feasibility of these systems. Closed-form expressions for key performance metrics, including QBER, sift probability, and Eve's error probability, have been derived using enhanced channel models that consider atmospheric attenuation, turbulence, and receiver noise. The study has presented numerical results to showcase the impact of various channel impairments on system performance. To improve overall performance, the study has also suggested optimal values for vital system setup parameters, including the receiver's aperture radius, the detector's threshold scale coefficient, and the transmit beam's divergence angle.

REFERENCES

[1] J. Ye, S. Dang, B. Shihada, and M.-S. Alouini, "Space-air-ground integrated networks: Outage performance analysis," *IEEE Trans. Wireless Commun.*, vol. 19, no. 12, pp. 7897–7912, Dec. 2020.

[2] N. Saeed, H. Almorad, H. Dahrouj, T. Y. Al-Naffouri, J. S. Shamma, and M.-S. Alouini, "Point-to-point communication in integrated satellite-aerial 6G networks: State-of-the-art and future challenges," *IEEE Open J. Commun. Soc.*, vol. 2, pp. 1505–1525, 2021.

[3] Y. Ai, A. Mathur, M. Cheffena, M. R. Bhatnagar, and H. Lei, "Physical layer security of hybrid satellite-FSO cooperative systems," *IEEE Photon. J.*, vol. 11, no. 1, pp. 1–14, Feb. 2019.

[4] V. Scarani, H. Bechmann-Pasquinucci, N. J. Cerf, M. Dušek, N. Lütkenhaus, and M. Peev, "The security of practical quantum key distribution," *Rev. Mod. Phys.*, vol. 81, pp. 1301–1350, Sep. 2009.

[5] S. Pirandola, U. L. Andersen, L. Banchi, M. Berta, D. Bunandar, R. Colbeck, D. Englund, T. Gehring, C. Lupo, C. Ottaviani, J. L. Pereira, M. Razavi, J. S. Shaari, M. Tomamichel, V. C. Usenko, G. Vallone, P. Villoresi, and P. Wallden, "Advances in quantum cryptography," *Adv. Opt. Photon.*, vol. 12, no. 4, pp. 1012–1236, 2020.

[6] A. Kumar and S. Garhwal, "State-of-the-art survey of quantum cryptography," *Arch. Comput. Methods Eng.*, vol. 28, pp. 3831–3868, Apr. 2021.

[7] M. Mehic, M. Niemiec, S. Rass, J. Ma, M. Peev, A. Aguado, V. Martin, S. Schauer, A. Poppe, C. Pacher, and M. Voznak, "Quantum key distribution: A networking perspective," *ACM Comput. Surv.*, vol. 53, pp. 1–41, Sep. 2020.

[8] A. Denys, P. Brown, and A. Leverrier, "Explicit asymptotic secret key rate of continuous-variable quantum key distribution with an arbitrary modulation," *Quantum*, vol. 5, p. 540, Sep. 2021.

[9] F. Kanitschar and C. Pacher, "Optimizing continuous-variable quantum key distribution with phase-shift keying modulation and postselection," *Phys. Rev. Appl.*, vol. 18, no. 3, Sep. 2022, Art. no. 034073.

[10] N. Hosseinidehaj, Z. Babar, R. Malaney, S. X. Ng, and L. Hanzo, "Satellite-based continuous-variable quantum communications: State-of-the-art and a predictive outlook," *IEEE Commun. Surveys Tuts.*, vol. 21, no. 1, pp. 881–919, 1st Quart., 2019.

[11] J. Yin, Y. H. Li, S. K. Liao, M. Yang, Y. Cao, L. Zhang, J. G. Ren, W. Q. Cai, W. Y. Liu, S. L. Li, and R. Shu, "Entanglement-based secure quantum cryptography over 1,120 kilometers," *Nature*, vol. 528, pp. 501–505, Jun. 2020.

[12] X. Ai and R. Malaney, "Optimised multithreaded CV-QKD reconciliation for global quantum networks," *IEEE Trans. Commun.*, vol. 70, no. 9, pp. 6122–6132, Sep. 2022.

[13] H. T. T. Phan, M. B. Vu, H. T. T. Pham, and N. T. Dang, "Satellite continuous-variable quantum key distribution systems using code-division multiple access," *Opt. Continuum*, vol. 2, no. 2, pp. 289–302, Feb. 2023.

[14] R. Bedington, J. M. Arrazola, and A. Ling, "Progress in satellite quantum key distribution," *NPJ Quantum Inf.*, vol. 3, no. 1, p. 30, Aug. 2017.
[15] M. Q. Vu, H. D. Le, T. V. Pham, and A. T. Pham, "Toward practical entanglement-based satellite FSO/QKD systems using dual-threshold/direct detection," *IEEE Access*, vol. 10, pp. 113260–113274, 2022.
[16] M. Q. Vu, T. V. Pham, N. T. Dang, and A. T. Pham, "Design and performance of relay-assisted satellite free-space optical quantum key distribution systems," *IEEE Access*, vol. 8, pp. 122498–122510, 2020.
[17] F. Fidler, M. Knapek, J. Horwath, and W. R. Leeb, "Optical communications for high-altitude platforms," *IEEE J. Sel. Topics Quantum Electron.*, vol. 16, no. 5, pp. 1058–1070, Sep. 2010.
[18] K. P. Peppas, G. C. Alexandropoulos, E. D. Xenos, and A. Maras, "The Fischer–Snedecor $\mathcal{F}$-distribution model for turbulence-induced fading in free-space optical systems," *J. Lightw. Technol.*, vol. 38, no. 6, pp. 1286–1295, Mar. 15, 2020.
[19] P. V. Trinh, N. T. Dang, and A. T. Pham, "All-optical relaying FSO systems using EDFA combined with optical hard-limiter over atmospheric turbulence channels," *J. Lightw. Technol.*, vol. 33, no. 19, pp. 4132–4144, Oct. 1, 2015.
[20] C. H. Bennett, G. Brassard, and N. D. Mermin, "Quantum cryptography without Bell's theorem," *Phys. Rev. Lett.*, vol. 68, no. 5, pp. 557–559, Feb. 1992.
[21] M. B. Vu, H. T. T. Pham, A. T. Do, H. T. T. Phan, and N. T. Dang, "Satellite-based free-space quantum key distribution systems using QPSK modulation and heterodyne detection receiver," in *Proc. 19th Int. Symp. Commun. Inf. Technol. (ISCIT)*, Sep. 2019, pp. 265–270.
[22] T. V. Nguyen, T. V. Pham, N. T. Dang, and A. T. Pham, "Performance of generalized QAM/FSO systems with pointing misalignment and phase error over atmospheric turbulence channels," *IEEE Access*, vol. 8, pp. 203631–203644, 2020.
[23] J. Li, Y. Yao, G. Wu, J. Hou, W. Yu, B. Liu, and J. Liu, "Broadband laser Doppler frequency shift emulator for satellite laser communication," *IEEE Photon. J.*, vol. 11, no. 6, pp. 1–12, Dec. 2019.
[24] T. V. Nguyen, H. D. Le, and A. T. Pham, "On the design of RIS–UAV relay-assisted hybrid FSO/RF satellite–aerial–ground integrated network," *IEEE Trans. Aerosp. Electron. Syst.*, vol. 59, no. 2, pp. 757–771, Apr. 2023.
[25] T. V. Nguyen, H. D. Le, N. T. Dang, and A. T. Pham, "Average transmission rate and outage performance of relay-assisted satellite hybrid FSO/RF systems," in *Proc. Int. Conf. Adv. Technol. for Commun. (ATC)*, Oct. 2021, pp. 1–6.
[26] O. S. Badarneh and R. Mesleh, "Diversity analysis of simultaneous mmWave and free-space-optical transmission over $\mathcal{F}$-distribution channel models," *IEEE/OSA J. Opt. Commun. Netw.*, vol. 12, no. 11, pp. 324–334, Nov. 2020.
[27] L. C. Andrews and R. L. Phillips, *Laser Beam Propagation through Random Media*, 2nd ed. Bellingham, WA, USA: SPIE Press, 2005.
[28] T. V. Nguyen, H. D. Le, N. T. Dang, and A. T. Pham, "On the design of rate adaptation for relay-assisted satellite hybrid FSO/RF systems," *IEEE Photon. J.*, vol. 14, no. 1, pp. 1–11, Feb. 2022.
[29] G. P. Agrawal, *Fiber-Optic Communication System*. Hoboken, NJ, USA: Wiley, 2002.
[30] Wolfram. (2023). *The Wolfram Functions Site*. [Online]. Available: http://functions.wolfram.com
[31] A. Prudnikov, Y. Brychkov, and O. Marichev, *Integrals, and Seriers: Volume 3: More Special Function*, vol. 3. London, U.K.: Gordon and Breach Science Publishers, 1986.
[32] V. S. Adamchik and O. I. Marichev, "The algorithm for calculating integrals of hypergeometric type functions and its realization in REDUCE system," in *Proc. Int. Symp. Symbolic Algebr. Comput.*, Jul. 1990, pp. 212–224.
[33] P. V. Trinh, T. V. Pham, N. T. Dang, H. V. Nguyen, S. X. Ng, and A. T. Pham, "Design and security analysis of quantum key distribution protocol over free-space optics using dual-threshold direct-detection receiver," *IEEE Access*, vol. 6, pp. 4159–4175, 2018.
[34] J. H. Shapiro, "Near-field turbulence effects on quantum-key distribution," *Phys. Rev. A, Gen. Phys.*, vol. 67, no. 2, Feb. 2003, Art. no. 022309.
[35] T. V. Pham, T. C. Thang, and A. T. Pham, "Average achievable rate of spatial diversity MIMO-FSO over correlated Gamma–Gamma fading channels," *J. Opt. Commun. Netw.*, vol. 10, no. 8, pp. 662–674, Aug. 2018.
[36] T. V. Nguyen, T. V. Pham, N. T. Dang, and A. T. Pham, "UAV-based FSO systems using SC-QAM signaling over fading channels with misalignment," in *Proc. IEEE 92nd Veh. Technol. Conf. (VTC-Fall)*, Nov. 2020, pp. 1–5.

THANG V. NGUYEN received the B.E. degree in electronics and telecommunications engineering from the Posts and Telecommunications Institute of Technology (PTIT), Vietnam, in 2017, and the M.E. and Ph.D. degrees in computer science and engineering from The University of Aizu (UoA), Japan, in 2019 and 2022, respectively. He is currently a Lecturer with PTIT. His current research interests include network modeling, performance analysis with a particular emphasis on space-air-ground integrated networks, optical wireless communications, quantum key distribution, hybrid FSO/RF systems, and intelligent reflecting surfaces. He received the IEEE ICCE Best Paper Award, in 2022.

HOA T. LE (Member, IEEE) received the B.E. degree in telecommunication engineering from the Posts and Telecommunications Institute of Technology (PTIT), Vietnam, in 2007, and the M.E. degree in telecommunication engineering from The University of Electro-Communications, Japan, in 2010. She is currently a Lecturer with the Faculty of Telecommunications 1, PTIT. Her research interests include non-terrestrial networks, optical wireless communications, VANET, vehicular communication, and cognitive radio.

HIEN T. T. PHAM received the B.E. degree from the University of Transport and Communications, Hanoi, in 1999, and the M.E. and Ph.D. degrees in telecommunication engineering from the Posts and Telecommunications Institute of Technology (PTIT), in 2005 and 2017, respectively. She has been with the Department of Wireless Communications, PTIT, since 1999. She is currently a Senior Lecturer with PTIT. Her research interests include design and performance evaluation of optical and wireless communication systems. She received the IEEE ISCIT Best Paper Award, in 2019.

VUONG MAI (Member, IEEE) received the Ph.D. degree in computer science and engineering from The University of Aizu (UoA), Japan. He is currently a Lecturer in electronics and communication engineering with the Faculty of Engineering and Informatics, University of Bradford, U.K. He is also a Core Team Member of the Bradford-Renduchintala Centre for Space AI. Prior to joining the University of Bradford, he was a Research Assistant Professor with the School of Electrical Engineering, KAIST, South Korea. His research interests include optical wireless, free-space optics, B5G/6G, aerial communications, and space communications.

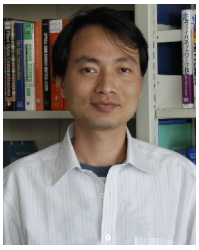

NGOC T. DANG (Member, IEEE) received the Ph.D. degree in computer science and engineering from The University of Aizu (UoA), Japan, in 2010. He is currently the Vice Dean of the Faculty of Telecommunications and the Head of the Department of Wireless Communications, Posts and Telecommunications Institute of Technology (PTIT), Vietnam. He is also an Associate Professor and the Head of the Wireless Systems and Applications Laboratory, PTIT. He was an Invited Researcher with the FOTON ENSSAT Laboratory, Université de Rennes 1, France, and a Research Fellow with the Laboratory of Computer Communications, UoA. His current research interests include the areas of communication theory with a particular emphasis on modeling, design, performance evaluation of optical CDMA, RoF, QKD, and optical wireless communication systems.